Journal of Materials Chemistry B

ROYAL SOCIETY OF CHEMISTRY

PAPER

View Article Online
View Journal

Cite this: DOI: 10.1039/d6tb00108d

Embedding near-infrared fluorescent single-walled carbon nanotubes within freeform fabricated hydrogels *via* continuous digital light processing

Alexander Boltinhouse,†[a] S M Abu Naser Shovon,†[b] Saroj Subedi,[b] Hussain Kawsar Chowdhury,[a] Henry Oliver Tenadooah Ware *[b] and Januka Budhathoki-Uprety *[a]

Received 13th January 2026,
Accepted 8th April 2026

DOI: 10.1039/d6tb00108d

rsc.li/materials-b

Photoluminescent single-walled carbon nanotubes (SWCNTs) are emerging materials for developing bioimaging agents and sensors. Free-standing architectures which include 3D printed freeform hydrogels can be leveraged as versatile platforms for sensors. However, a key challenge in developing 3D-printed SWCNT-based optical probes and sensors is preserving their optical properties under demanding processing conditions, such as UV irradiation and *in situ* free radical polymerization used in 3D printing processes. This research leveraged a continuous digital light processing (CDLP) technique to fabricate fluorescent SWCNT-embedded freeform hydrogels. We found that integrating an aqueous suspension of SWCNTs did not inhibit the creation of 3D fabricated hydrogel objects. However, the photoluminescence of SWCNTs in 3D-printed objects was adversely impacted by the SWCNT functionalization type, hydrogel ink formulations, and the process parameters during CDLP. Upon screening the formulation and the CDLP conditions, we identified that SWCNTs non-covalently functionalized with poly(styrene-*co*-styrene sulfonate) (PS-*co*-PSS) maintained their characteristic NIR emission in the 3D printing ink formulation and upon exposure to the UV-curing process. More importantly, no apparent leaching of SWCNTs was observed after two weeks of soaking in deionized water. By tuning the hydrogel ink formulation, structures with desirable application-specific properties could be achieved, such as the hydrogel 9–70 composition (9 wt% crosslinker-to-monomer ratio and 70 wt% water) exhibiting stretchability increase of up to ~142%. Both the hydrated and the dehydrated samples of key hydrogel ink formulations showed no evidence of cracking after 24 hours. This successful integration of NIR fluorescent SWCNTs into complex, freeform hydrogel architectures *via* CDLP represents a fundamental advance toward creating robust, portable, and versatile optical sensing platforms.

Introduction

Semiconducting single-walled carbon nanotubes (SWCNTs) have outstanding photophysical properties, which include non-photobleaching near infrared emission which is capable of penetrating light through biological tissues and producing optical responsiveness to changes within the SWCNT environment, making these materials well suited for bioimaging and sensing applications.[1,2] However, pristine SWCNTs require de-bundling and functionalization to render SWCNTs soluble in chosen solvents, harness the optical properties of SWCNTs, and facilitate molecular interactions with their targets. Common approaches to functionalizing SWCNTs include non-covalent functionalization methods which can occur under mild conditions with minimal impact on the SWCNT's intrinsic optical properties, and the surface can be functionalized *via* tunable biocompatible materials.[3] The non-covalent surface modification of SWCNTs usually takes advantage of hydrophobic interactions and π–π stacking of dispersant compounds with the graphitic surface of SWCNTs.[4–7] Several different types of compounds including DNA,[8] surfactants,[9–11] and synthetic polymers[7,12,13] have been explored for SWCNT surface functionalization. The optical sensing capabilities of SWCNTs arise from their distinct band-gap fluorescence.[14,15] When photoexcitation occurs in a SWCNT, the resulting exciton (electron–hole pair) migrates along the carbon lattice and eventually recombines, resulting in near-

[a] *Department of Textile Engineering, Chemistry and Science, North Carolina State University, Raleigh, NC, 27695, USA. E-mail: jbudhat@ncsu.edu*
[b] *Department of Mechanical and Aerospace Engineering, North Carolina State University, Raleigh, NC, 27695, USA. E-mail: howare@ncsu.edu*
† These authors contributed equally.

infrared (NIR) emission.[15,16] Changes in the immediate environment on the SWCNT surface affect the exciton dynamics and cause shifts in emission intensity or wavelength. Such optical changes can result from direct interaction with an analyte or change in pH, temperature, solvent dielectrics and redox reactions that affect the SWCNT photoluminescence.[3]

While the majority of research studies on photoluminescent SWCNTs have focused on solution-based strategies, it is crucial to develop methods to incorporate SWCNTs into various platforms to produce targeted optical probes and sensors for their applications in complex geometry surfaces and as implantable/wearable devices.[17] In this regard, SWCNTs have been integrated into fibers/flexible substrates,[18,19] hydrogel materials,[20] and conductive films and printed surfaces.[21–24] Chemically mild formulations and processing techniques seemed to retain the optical properties of SWCNTs incorporated into solid substrates. For instance, DNA-functionalized SWCNT suspensions that showed optical responses to hydrogen peroxide, a marker of oxidative stress, retained their sensing ability even when these SWCNTs were encapsulated within optical core–shell microfibrous textiles.[18] Similarly, the functionalized SWCNTs which exhibited optical responses to glucose, retained this optical sensing ability when the SWCNT suspension was converted into a hydrogel matrix under mild conditions.[25] Sodium cholate (SC) and sodium dodecyl sulfate (SDS) were used to disperse (6,5) SWCNTs which were then mixed with a polyvinyl alcohol (PVA) solution. Apoglucose oxidase, an enzyme which converts glucose into oxygen, was used to crosslink PVA into a hydrogel.[25] The PVA–SWCNT hydrogel was implanted subdermally in a mouse model, exposed to 10 mM glucose, and the response was measured. It was shown that the response to glucose was not affected by the implantation.[25]

Hydrogels are three-dimensional polymer networks based on covalently cross-linked hydrophilic polymers, which allow them to retain water within their network with tunable mechanical properties and without compromising structural integrity.[17] The integration of SWCNTs into optical probes and sensors embedded within hydrogels and other polymer matrices represents a transformative approach in advancing sensing technology.[25,26] However, conventional hydrogel fabrication methods provide limited control over spatial distribution, restricting the ability to create complex, heterogeneous sensing networks.[27] Additive manufacturing (AM, also known as 3D printing) represents an approach to overcome these traditional limitations with AM's ability to create objects layer-by-layer and unlock greater geometric complexity. AM enables the fabrication of complex or customized structures, which would be difficult or impossible *via* traditional manufacturing methods.[28] This is especially significant for soft materials such as hydrogels. The two most common 3D printing methods which work with hydrogels are direct ink writing (DIW) and vat photopolymerization (VPP) processes.

DIW prints objects *via* extrusion and is one of the most versatile AM methods in terms of printing materials, making it one of the most widely used approaches. DIW, however, requires the printing ink to exhibit viscoelastic "shear thinning" behavior with relatively high viscosity (10^3–10^6 mPa s).[29,30] In DIW, most chosen hydrogels exhibit the necessary viscosity range, but are generally mixed with different additive fillers (micro or nanoparticles) to either obtain the required rheological properties or to add functional behaviors to the print. DIW has been successfully utilized to print ionically conductive hydrogels and conductive composites for sensors and other functional products.[31,32] Geometric complexity can be limited within DIW due to the deposition working principle and the single nozzle deposition compared to other methods. For example, stand-alone 3D structural features with very high resolution ($\leq$200 μm), seen in objects such as lattices, are challenging to print *via* DIW.[33,34] Vat photopolymerization (VPP) utilizes a light source to selectively cure the liquid photosensitive ink contained in the vat to fabricate 3D structures.[35] Within VPP, the surrounding liquid ink can act as a natural, passive support for more complex geometries compared to deposition methods. VPP is a family of processes which include stereolithography (SLA), digital light processing (DLP), and more recently "Continuous" DLP (CDLP). DLP has been successfully used to print hydrogel-based multi-modal sensors like strain sensors,[36] capacitive sensors,[37] or tactile sensors,[38] which have been developed for human health monitoring. Recently, CDLP has gained increasing attention due to its high resolution (1 μm to 200 μm) and rapid printing speed, achieving 100—1000 s of mm per hour printing speed, made possible *via* its continuously moving build platform during printing.[33,35] To the authors' knowledge, there has not been any report of photoluminescent SWCNTs as optical sensors embedded within true freeform fabricated hydrogels.

While VPP methods such as DLP and CDLP can be advantageous in terms of geometric complexity, resolution, and fabrication speed, sensitive materials will be subjected to potentially demanding processing conditions, which include material exposure to UV-curing and *in situ* free radical photopolymerization for the polymer substrate. These conditions could adversely impact SWCNT photoluminescence unless the nanotube surface is protected *via* functionalization. 3D printing methods, like CDLP, pose challenges for optical/fluorescence sensor platforms due to the sensors' exposure to UV irradiation and interactions with the ink ingredients such as photoinitiators, reactive monomers and cross-linking agents, which could deter photoluminescence of the embedded functionalized SWCNTs. However, protective surface coverage on SWCNTs could preserve their optical properties. Here, we leverage CDLP technology to develop soft architectures with embedded optically active SWCNTs (Fig. 1). This research addresses a critical challenge through successfully embedding NIR fluorescent SWCNTs within true freeform fabricated hydrogels using CDLP technology.

Experimental section

Materials

SWCNTs consisting of $\geq$77% (7,6) chirality (product #704121), polyvinyl pyrrolidone (PVP) ($M_w \approx 40\,000$ g mol^{-1}), sodium cholate (SC), dimethyl sulfoxide (DMSO), poly(ethylene glycol) diacrylate (M_n 700 Da, PEGDA), poly(ethylene glycol) methyl ether acrylate (M_n 480 Da, PEGMEA), phenylbis(2,4,6-trimethylbenzoyl)

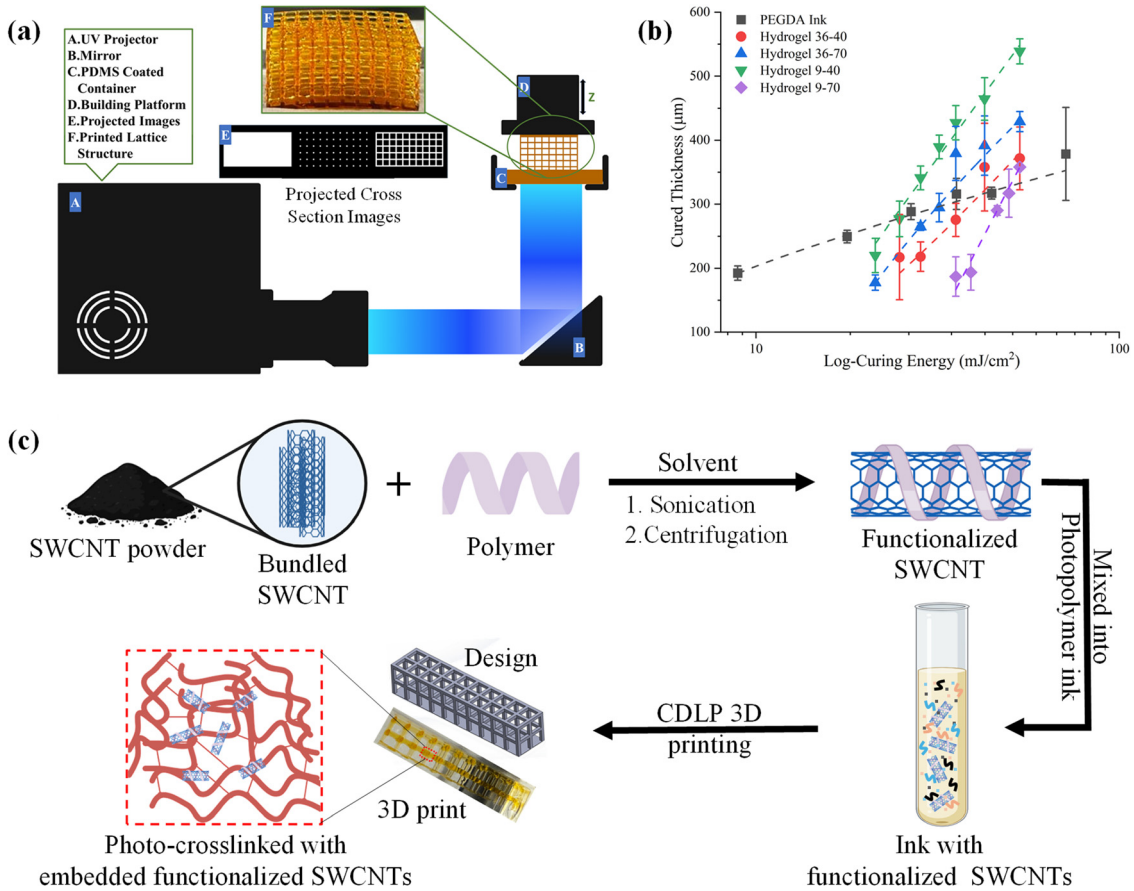

Fig. 1 (a) Schematic diagram of the printing process. (b) Curing curve for PEGDA ink and all hydrogel inks used in this study. (c) Our approach to functionalized SWCNTs and embedding nanotubes into 3D printed hydrogel substrates.

phosphine oxide (Irgacure 819, photoinitiator) lithium phenyl-2,4,6-trimethylbenzoylphosphinate (LAP, photoinitiator) and Triton-X 100 were purchased from Sigma Aldrich, St. Louis, MO, United States. Poly(styrene-*co*-styrene sulfonate) (PS-*co*-PSS), in sodium salt form with a degree of sulfonation >13 mol%, was purchased from Polymer Source Inc., Montreal, Canada. Orasol dye (Orange G) was purchased from MuseuM Services Corporation, South St. Paul, MN, United States. Deionized and distilled water was used for sample preparation.

Instruments

UV-Vis-NIR spectroscopy. SWCNT samples were characterized using a UV-vis-NIR spectrophotometer (Agilent Cary 5000).

NIR fluorescence spectroscopy. NS MiniTracer (Applied NanoFluorescence, LLC, TX, USA) was used to measure NIR fluorescence from the SWCNT samples.

General method for preparing suspensions of SWCNTs

SWCNT suspensions were prepared by adding 1 mg of SWCNTs to deionized (DI) water containing surfactant or polymer. The solution concentrations of the dispersants were 5 mg mL^{-1} for poly(vinylpyrrolidone) (PVP), 10 mg mL^{-1} for sodium cholate (SC), and 20 mg mL^{-1} for poly(styrene-*co*-styrene sulfonate). A centrifuge tube with 1 mg of SWCNT powder and 1 mL of the suspending agent solution was placed in a cold tube rack. The mixture was sonicated using an FB-505 ultrasonic liquid processor (Fisher Scientific) at 20% amplitude in pulsed mode (30 s on, 30 s off) for 10 minutes (total 20 minutes), followed by centrifugation at 14 000 rpm for 30 minutes using a Sorvall Legend Micro 21 centrifuge (Thermo Scientific). The supernatant was collected and diluted with deionized water to 1 mL total volume, then subjected to a second centrifugation cycle with the same parameters (14 000 rpm for 30 minutes). If using a polymer suspending agent, the SWCNT solution is filtered using a centrifugal membrane filter of 100 kDa MWCO (Millipore Sigma), at 14 000 rpm for 7 minutes. The concentrate was collected and diluted as needed in DI water prior to characterization by UV-Vis-NIR absorbance and NIR photoluminescence spectroscopies. The general procedure of creating the functionalized SWCNTs is shown in the top portion of Fig. 1c.

Characterization of SWCNT suspensions

The PS-*co*-PSS-SWCNT suspension was characterized using UV-vis-NIR absorbance and NIR fluorescence measurements. The concentration of SWCNTs in the aqueous suspension was determined using the absorbance value at 626 nm and using the SWCNT coefficient of 0.036 L mg^{-1} cm^{-1} as reported previously.[11] The fluorescence was measured at an integration

value of 5000 and with an averaging of 3. DI water was used as a reference for both absorbance and fluorescence measurements.

NIR fluorescence measurements on printed objects

The 3D printed hydrogel structures were rinsed with DI water twice and placed individually in cuvettes (polystyrene 4.5 mL cuvette) and filled with DI water prior to fluorescence measurements. A blank hydrogel, which is a hydrogel structure with no SWCNTs within the structure, was used as the reference. An integration value of 5000 and an averaging of 3 were used for measurements. This method was used for both printed complex 3D structures and flat structures.

CDLP 3D printing

In this work, a custom-built CDLP printing setup was used for 3D printing the hydrogels and the SWCNT-infused hydrogel objects. A UV light source (LRS-4KA 4 K UV Projector, Keynote Photonics) with a high resolution of 1528 × 2716 pixels (~10.8 μm pixel size) projected UV light of a wavelength of 385 nm. A borosilicate glass Petri dish was used as an ink container. The Petri dish was coated with polydimethylsiloxane (10 : 1, PDMS : Hardener ratio) and silicon oil (30 wt% with viscosity of 100 mPa s) to reduce adhesion during the printing process.[39] More details on the printer setup can be found in our previously published work.[40] The 3D design, modeled by SolidWorks, was sliced into a series of 2D images *via* the CHITUBOX slicing software. In DLP printing, the UV projector projects 2D images layer by layer onto the surface of the photosensitive resin ink, initiating photopolymerization. The cured structure gets printed out along the movement of the *Z*-axis build platform driven by a motorized stage (X-LSQ075A-E01, Zaber Technologies) (Fig. 1a).[41] A custom-made LabVIEW program controls both the projection and the stage movement. The ''Continuous'' DLP (CDLP) process was used for all hydrogel specimen printing. The non-stick nature of the silicone oil-infused PDMS coating enables the printer's built platform to move continuously while the light is dynamically projected onto the ink surface, eliminating the need for pauses between individual layer fabrication sequences that are characteristic of standard DLP printing.[35,42] After printing, PEGDA and Irgacure 819-based structures were rinsed in ethanol for 5 minutes to remove any uncured ink from the printed surface. As the uncured hydrogel ink is water soluble, the printed hydrogel structures were submerged in distilled water for an hour to clean the uncured ink from the printed surface before performing characterization and measurement.

Preparation of printable inks

The first UV-curable ink in this study was prepared using a combination of PEGDA and Irgacure 819 at a concentration of ~2.2 wt% of PEGDA (hereafter known as Pure PEGDA). The mixture was sonicated *via* a Branson 2800 bath sonicator for one hour at 50 °C before using it in the printing system. Bath sonication was used to ensure a relatively rapid dissolution of photoinitiator powders into our respective inks. The hydrogel inks were developed using the combination of PEGMEA, distilled water, PEGDA, Orasol dye solution, Triton X-100 surfactant and LAP photoinitiator. Crosslinker PEGDA and monomer PEGMEA were mixed at two concentration ratios to each other: 36 wt% and 9 wt%. Additionally, the distilled water concentration was varied between ~40 wt% and ~70 wt% in hydrogel ink. Combining the variations of crosslinker, monomer, and distilled water, four distinct hydrogel formulation inks were investigated, which are denoted as hydrogel 36–40, 36–70, 9–40, and 9–70 (Table 1). The remaining ink components were kept constant in all four-hydrogel inks. Orasol dye solution and LAP photoinitiator were mixed at 3.5 wt% and 0.8 wt% of the total weight of PEGMEA, PEGDA and distilled water. The Orasol dye solution was prepared using 1 wt% dye dissolved in ethanol. Surfactant Triton-X 100 was mixed in the mixture at 50 wt% of Orasol dye concentration, and this helps the dye to distribute in the hydrogel ink evenly. After mixing all the components, we sonicated the mixture for 60 minutes at 25 °C before using the ink for 3D printing. The sonication and the final prepared inks were maintained in a light-protected environment to avoid any unintended polymerization of the ink monomers.

Preparation of SWCNT-infused inks

All three functionalized SWCNT types (SC-SWCNT, PS-*co*-PSS-SWCNT, and PVP-SWCNT) were suspended in DI water as described in prior sections and the nanotube suspensions were mixed at constant 10 vol% within the pure PEGDA ink and within a chosen hydrogel formulation (Table 2). Note that the initial concentration of SWCNTs in each functionalization type varied to allow measurable photoluminescence in the nanotube suspension. To evenly distribute the SWCNT suspension, the mixture was sonicated for three minutes using Fisher Scientific™ Model 705 Sonic dismembrator with 10% amplitude and 15 W power. After every 60 seconds of sonication, the sonication was paused for 30 seconds to mitigate excessive temperature rise of the composite SWCNT-hydrogel inks. The incorporation of the functionalized SWCNTs into the matrix is pictorially represented in Fig. 1c.

Table 1 Hydrogel formulation with concentration details. In terms of naming details, the 1st number in the formulation name represents the crosslinker-to-monomer ratio (%) and the 2nd number is the rounded distilled water concentration (%)

	Concentration in wt%						
Formulation details	PEGMEA	Distilled water	PEGDA	LAP	Orasol dye solution	Triton-X 100	Total weight
Hydrogel 36–40	41.48	37.71	15.08	0.75	3.33	1.63	100.00
Hydrogel 36–70	21.31	68.01	4.79	0.78	3.43	1.68	100.00
Hydrogel 9–40	50.46	36.65	7.33	0.73	3.24	1.59	100.00
Hydrogel 9–70	25.96	66.00	2.33	0.75	3.33	1.63	100.00

Table 2 Formulation details of functionalized SWCNT composites, unless otherwise noted for the specific experiment

Formulation details	Photopolymer ink	Infused functionalized SWCNT	Concentration of functionalized SWCNT suspension in ink
PVP-SWCNT-infused PEGDA composite	Pure PEGDA	PVP-SWCNT	10 vol%
SC-SWCNT-infused PEGDA composite		SC-SWCNT	
PS-*co*-PSS-SWCNT-infused PEGDA composite		PS-*co*-PSS-SWCNT	
PS-*co*-PSS-SWCNT-infused hydrogel composite	Hydrogel 36–40	PS-*co*-PSS-SWCNT	
	Hydrogel 36–70		
	Hydrogel 9–40		
	Hydrogel 9–70		

Curing characterization

The tested inks' cured thickness (C_D) was measured with respect to input energy (E_{max}) and fitted according to the Beer–Lambert Law relationship, known as the "Working Curve" which can be expressed as:[43,44]

$$C_D = D_p \ln\left(\frac{E_{max}}{E_c}\right)$$

where the variables include critical energy (E_c), depth of penetration (D_p) and the emitted light energy (E_{max} = light intensity × exposure time). E_c is the minimum energy required to initiate the photopolymerization, D_p is the depth at which the light intensity reduces to $1/e$ (e is the Euler number) in the ink and E_{max} is the emitted light energy applied to the surface of the ink. E_c and D_p are ink-specific properties, whereas E_{max} is user-controlled. To experimentally measure different inks' cured thickness, we applied a constant 3.32 mW cm^{-2} light intensity over a 1000 px × 2600 px area (10.8 mm × 28.1 mm) and varied the exposure time to cure a rectangular solid volume for thickness measurement. With a constant light intensity, the emitted light energy (E_{max}) changes with the variation of exposure time. We cured flat rectangular solids in 5–7 different emitted light energies (E_{max}). The cured thickness (C_D) was measured over 6 different locations on every rectangular solid *via* a digital micrometer and averaged. From the logarithmically fitted working curve and Beer–Lambert Law relationship, we estimated the depth of penetration (D_p) from the slope of the curve. We estimated *via* curve extrapolation the critical energy (E_c), where the cured thickness begins (C_D = 0, the X-axis intercept of the working curve) shown in Fig. S2.

FTIR measurements on hydrogels and the hydrogel ink without curing

Fourier transform infrared (FTIR) spectroscopy was performed in neat hydrogel and PS-*co*-PSS SWCNT-infused hydrogel of all four formulations. The FTIR was measured in both "UV-Cured" and "Uncured" conditions of hydrogels. For "Uncured" conditions, the prepared neat and SWCNT-infused hydrogel suspension inks were directly used. To prepare "UV-Cured" samples, we applied a constant 3.32 mW cm^{-2} light intensity over a 1000 px × 2600 px area (10.8 mm × 28.1 mm) with 15 s exposure time to cure flat rectangular objects for FTIR measurements. An FTIR spectrophotometer (Thermo Fisher Scientific, Nicolet™ iS™ 10) was used to analyze all samples. The spectra were generated using 32 scans with a resolution of 4 cm^{-1} in the 4000 to 400 cm^{-1} spectral window. All prepared inks and UV cured samples were characterized with FTIR analysis without additional sample preparation.

To investigate crosslinking *via* UV curing we measured the characteristic peak associated with the vinyl group (C═C double bond, ~1638 cm^{-1})[45] and measured the reduction of this absorption peak between ink formulation and UV-cured solid. Reduction in C═C double bonds was calculated *via* the following equation:

$$\text{Reduction}_{C=C} = \left(1 - \frac{A_{cured,C=C}}{A_{uncured,C=C}}\right) \times 100$$

where the A terms represent the measured absorption at the characteristic C═C peak. A_{cured} and $A_{uncured}$ represent the measured absorption value for the solid samples and the uncured ink, respectively.

Mechanical characterization

Tensile testing was carried out following the American Society for Testing and Materials (ASTM) D638 standard in dog bone shaped samples at a 4 mm min^{-1} strain rate in a universal testing machine (Instron – 2580-5 kN/164487) with a 5 kN load cell. The tensile testing was performed following ASTM D638 standard of Type V dog bone shaped samples (specimen length: 40 mm, gage region: W3 mm × T3 mm).[46] The tensile specimen designs were slightly modified to include semi-spherical texture on the grip regions to enable more repeatable tensile testing and higher instances of intended failure within the gage region.

Hydrogel swelling characterization

The swelling measurement was performed with hydrogel 36–40 with the same size (8 mm^3) of solid and lattice cube. We observed both the volume and weight increase of the solid and lattice cubes every 10 minutes for an hour. The swelling rate was determined using the following equations:

$$\text{Volume swelling increase} = \left(\frac{V_S - V_{AP}}{V_{AP}}\right) \times 100$$

$$\text{Weight swelling increase} = \left(\frac{W_S - W_{AP}}{W_{AP}}\right) \times 100$$

where V_S or W_S is the volume or weight of the swollen hydrogel and V_{AP} or W_{AP} is the volume or weight of the as-printed hydrogel, respectively.

Viability/durability test of hydrogels

We conducted viability/durability tests on the unfilled hydrogel ink formulations (no added SWCNTs) denoted in Table 1. For any designed structure it is very important that the fabricated design remains viable throughout the intended application. If the printed structures are not able to maintain their intended form without cracks or full structure failure, then these represent a non-viable or fragile object and are unsuitable for the intended application. Hydrogels represent a material which can significantly increase in volume due to intake or release of water due to hydration or dehydration. This test was performed as a qualitative assessment on the potential cracking behavior in 3D prints subjected to initially "Hydrated" or "Dehydrated" conditions and finally to "Reversed" conditions. To conduct the viability/durability test, rectangular flat structures were 3D printed with the various ink formulations in neat-hydrogel (Fig. S3) and SWCNT-infused hydrogel (Fig. S4). The structures were either stored submersed in distilled water (hydrated condition) or allowed to dry in ambient air (dehydrated condition) for 24 hours before observation. Following the 24 hour period, the sample structures' surfaces were visually inspected. After determining the hydrogel's cracking behavior in its initial handling conditions, we next switched the sample's original handling condition ("Reversed" condition, *i.e.* switch from hydrated-to-dehydrated conditions or *vice versa*). The samples in the reversed condition were allowed to acclimate in their new environment for 24 hours. We evaluated whether the structures were fully intact to determine their cracking nature in both the hydrated and the dehydrated conditions.

Results and discussion

Curing characterization

Initial curing characterization for printability of the various ink formulations utilized the hydrogel 36–40 formulation, with varying concentration of Orasol Orange G dye within the ink. Addition of Orasol Orange G dye did significantly attenuate the incident light and subsequent curing. Working curves for all tested Orasol concentrations are shown in Fig. S1. The hydrogel 36–40 ink with 0.5 wt% Orasol dye showcased very large D_p (872.58 μm), which was too large to enable high-resolution 3D printing. Also, the steeper curing curve with 0.5 wt% indicates that a small energy change can significantly increase the curing thickness, making layer-by-layer printing difficult. We gradually increased the Orasol dye percentage to reduce D_p to become much closer to our intended layer height in 3D printing. With ~3.5 wt% and ~4.5 wt% Orasol dye, we observed similar results. Therefore, we have finalized ~3.5 wt% Orasol dye for all subsequent hydrogel ink formulations. For the hydrogel ink with ~3.5 wt% Orasol dye, the depth penetration (D_p) was 233.51 μm, and critical energy (E_c) was 10.35 mJ cm^{-2} (Fig. S1 and Table S1).

Furthermore, we additionally characterized the curing behavior of pure hydrogel formulations denoted in Table 1 at ~3.5 wt% dye with varying crosslinker-to-monomer ratios and water concentrations in the hydrogel inks. We observed an increase in D_p in all three hydrogel formulations including hydrogel 36–70 (286.56 μm), hydrogel 9–40 (346.52 μm), and hydrogel 9–70 (443.43 μm) compared to the hydrogel 36–40 formulation due to the reduction of cross-linking density. Also, the critical energy E_c didn't change significantly with hydrogel 9–40 (10.87 mJ cm^{-2}) and hydrogel 36–70 (11.03 mJ cm^{-2}) formulations, but in the hydrogel 9–70 formulation E_c significantly increased to 24.11 mJ cm^{-2} (Fig. 1b). Furthermore, we also characterized the curing behavior of pure PEGDA ink and observed an 86.88 μm depth of penetration (D_p) and 0.985 mJ cm^{-2} critical energy (E_c).

Hydrogel swelling characterization

The measured swelling rate of solid hydrogel cubes was relatively low compared to the cubic lattice structures due to their low surface area open to water. The lattice structures' swelling becomes effectively constant after 10–20 minutes. Of importance, which arose during the swelling characterization, was that the solid cubes (made from the hydrogel 36–40 formulation) tended to crack, which we hypothesize is due to the osmosis pressure difference of the water surrounding the hydrogels. This fact ultimately convinced us to pursue durability testing for all subsequent hydrogel formulation characterization. When measuring swelling rates (the slope in both sample types due to swelling, Fig. 2) over 20 minutes, we observed approximately 2× higher slopes (swelling per min) in volume swelling (cubic lattice – 4.82; solid cube – 2.39) and weight swelling (cubic lattice – 3.17; solid cube – 1.64) with the lattice structures compared to solid structures.

Viability/durability test of hydrogels

To investigate the influence of water content and crosslinker-to-monomer ratio before complex geometry 3D printing, we observed the cracking due to the volume change of the hydrogels (Fig. S3). The "Durability" we defined as rating the structures' viability in both hydrated and dehydrated conditions with no presence of cracks in the samples. Hydrogel formulations which could not survive in either hydrated or dehydrated conditions, we denoted as "Fragile" samples. The viability durability test was first performed with neat hydrogels and subsequently within SWCNT-infused hydrogels. The durability ranking of each formulation was set by the behavior of the neat hydrogels. The "Highly Durable" formulations could undergo both hydrated, dehydrated, and reversed conditions without cracking. Fragile behavior was clearly observed in low water-containing hydrogel inks. Hydrogel 36–40 was observed to be the "Most Fragile" of all formulations, with evident breakage/cracking under hydrated conditions after swelling in water for 24 hours. This formulation also cracked under dehydrated conditions, which indicates its nonviability for most applications. Due to cracking observed in both hydrated and dehydrated conditions, this formulation was not subjected to reverse conditions. The other reduced water (~40 wt% water hydrogel ink formulation) hydrogel 9–40 showed evidence of fracture/cracking under dehydrated conditions but survived under hydrated conditions for the 24 hours. Hydrogel 36–70 and hydrogel 9–70 exhibited much more durable natures than the formulations containing a lower water concentration in both hydrated and dehydrated conditions with no presence of

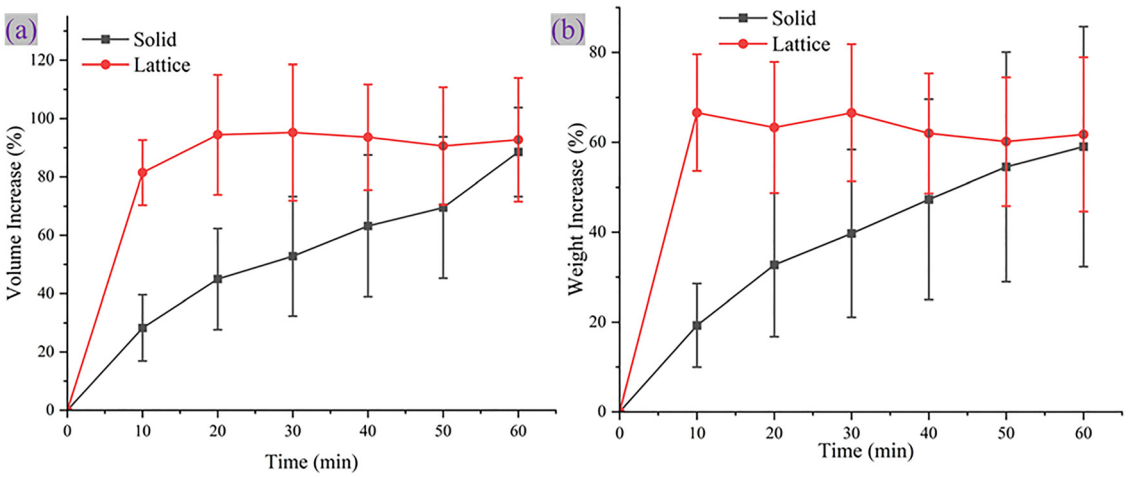

Fig. 2 Swelling by volume (a) and weight (b) of solid and lattice hydrogel 36–40.

cracks/fracture. Therefore, after 24 hours, these formulations were next subjected to reversed conditions. Upon subjecting the samples to reversed conditions, we observed cracking behavior in hydrogel 9–40 only. Hydrogel 9–40 exhibited cracking when switched from initially hydrated to 24 hour dehydrated conditions. However, the structures made with hydrogel 36–70 and hydrogel 9–70 were equally denoted as highly durable having exhibited no cracking under hydrated, dehydrated, or reversed conditions.

The addition of SWCNTs into the hydrogel formulations did notably improve the durability of the initially fragile hydrogel formulations. In the SWCNT-infused hydrogels, all formulations survived in both the initial hydrated and initial dehydrated conditions after printing with no presence of cracks/fracture. In contrast to the neat hydrogels, all samples could undergo reverse conditions. However, under 24 hour reversed conditions, cracking behavior was observed only in the switch to dehydrated conditions from initially hydrated conditions in the SWCNT-infused hydrogel 36–40 and 9–40 (Fig. S4). The SWCNT-infused hydrogel 36–70 and 9–70 exhibited durable nature in both initial hydrated and dehydrated environments, as well as the 24 hour reversed conditions. Table 3 highlights the durability rankings of the tested hydrogel formulations.

Pure PEGDA ink and hydrogel mechanical characterization

The pure PEGDA ink and all developed hydrogels exhibited a wide variation of mechanical properties based on the ink formulation. Pure PEGDA showed eight times higher Young's modulus (12.27 MPa) compared to the closest hydrogel formulation 36–40 (1.69 MPa) most likely due to a high crosslinking density property of PEGDA.[47] Mechanical toughness is attributed to the material's ability to absorb maximum energy before ultimate failure. This property is valuable as it takes into account both the strength of the material, as well as its stretchability. Due to the high ultimate tensile strength (UTS) of pure PEGDA ink (5.67 MPa), the overall toughness of the PEGDA ink (1440 kJ m^{-3}) is significantly higher than all four hydrogel compositions ($\leq$179.98 kJ m^{-3}). However, the stretchability in PEGDA ink is relatively low (50.7%) compared to most of the hydrogel formulations. Significantly, hydrogel 36–40 exhibited the lowest stretchability (35%) of all tested inks. Moreover, pure PEGDA ink and hydrogel 36–40 exhibited fragile behavior due to significant changes in volume during swelling when immersed in water for 24 hours. Increasing the water concentration or reducing the amount of crosslinker (PEGDA) inside the hydrogel inks can resolve this issue. However, these approaches will reduce the overall crosslink density (and correspondingly the material's

Table 3 Hydrogel durability ranking. ✗ denotes cracking and ✓ denotes the viability of hydrogel samples in their corresponding environments. The "Initial" columns denote the initial 24 hour exposure to a specific environmental condition. The "Reverse" columns denote that the given samples survived the initial 24 hour environmental condition (*i.e.* hydrated) and were subjected to 24 hour exposure to the opposite environmental condition. For example, the reverse column under the hydrated heading denotes a hydrated-to-dehydrated environmental switch, and a reverse column under the dehydrated heading denotes a dehydrated-to-hydrated environmental switch

	Neat hydrogel				SWCNT-infused hydrogel				
	Hydrated survival		Dehydrated survival		Hydrated survival		Dehydrated survival		
Formulation details	Initial	Reverse	Initial	Reverse	Initial	Reverse	Initial	Reverse	Durability ranking (based on neat hydrogels)
Hydrogel 36–40	✗	N/A	✗	N/A	✓	✗	✓	✓	Most Fragile
Hydrogel 36–70	✓	✓	✓	✓	✓	✓	✓	✓	Highly durable
Hydrogel 9–40	✓	✗	✗	N/A	✓	✗	✓	✓	Fragile
Hydrogel 9–70	✓	✓	✓	✓	✓	✓	✓	✓	Highly durable

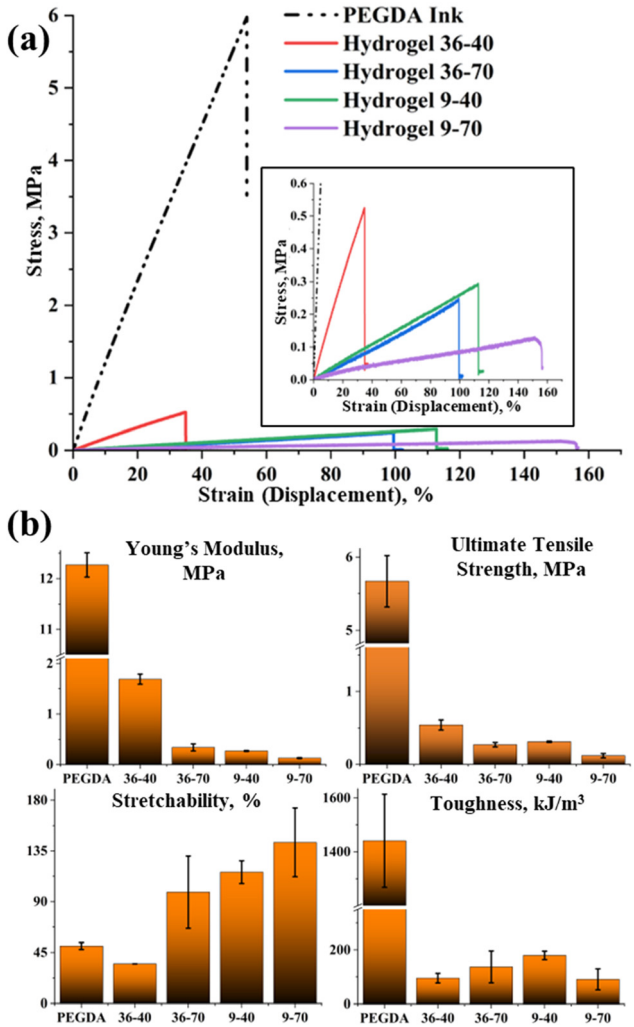

Fig. 3 (a) Stress–strain curve of different hydrogel composition; (b) comparison of ultimate tensile strength, Young's modulus, stretchability and toughness in different hydrogel compositions.

Young's modulus) as well as the strength (UTS) of the printed hydrogels.

Hydrogel formulations with water inclusion of 70 wt% significantly reduced the crosslinking density of the hydrogels, which correspondingly reduced the UTS and Young's modulus compared to those of hydrogel 36–40 (Fig. 3b). For example, we measured UTS of 0.27 MPa, 0.31 MPa, and 0.12 MPa in hydrogel 36–70, hydrogel 9–40, and hydrogel 9–70 hydrogels, respectively, compared to the high UTS in hydrogel 36–40 hydrogel (0.54 MPa). The Young's modulus was measured to be 0.34 MPa in hydrogel 36–70, 0.27 MPa in hydrogel 9–40, and 0.13 MPa in hydrogel 9–70 compared to the value of 1.69 MPa for hydrogel 36–40. The reduced crosslinking density increases the free volume within the polymer network enabling increased stretchability to extend their polymer chains, which ultimately increases the stretchability of the hydrogels.[48] Hydrogel 9–70 exhibited the highest stretchability (~142%) among all hydrogel compositions. The low mechanical toughness of the hydrogels leads to faster crack propagation and stress concentration that limits their practical applications.[49,50] Hydrogel 36–40 leads in terms of the UTS and Young's modulus among all hydrogel formulations. However, when considering the UTS and stretchability, we observed that Hydrogel 9–40 showed the highest mechanical toughness (179.98 kJ m^{-3}) among all the hydrogels.

SWCNT-infused-PEGDA and hydrogels and their optical properties

Aqueous dispersions of SWCNTs – SC-SWCNTs, PVP-SWCNTs, and PS-*co*-PSS-SWCNTs were added into printing ink formulations for the initial testing of printability. All tested SWCNT suspensions appear to be incorporated into the printed structures. However, SC-SWCNTs and PVP-SWCNTs showed little to no measured fluorescence signal from SWCNTs in the printed structures obtained from the PEGDA ink formulations (Fig. 4a and b).

To understand possible causes of fluorescence quenching factors, like exposure to UV light and potential photochemical damage during crosslinking reactions, effects from each major step in the manufacturing/development sequence were carefully examined individually. SC-SWCNT (~125 mg L^{-1}, initial concentration prior to mixing with printing ink) and PVP-SWCNT (~250 mg L^{-1}, initial concentration prior to mixing with printing ink) aqueous suspensions were added into the PEDGA sample at a ratio of about 1 : 5 (by volume), mixed with a pipette, and the NIR fluorescence was measured during this and subsequent steps. Note that the concentration of

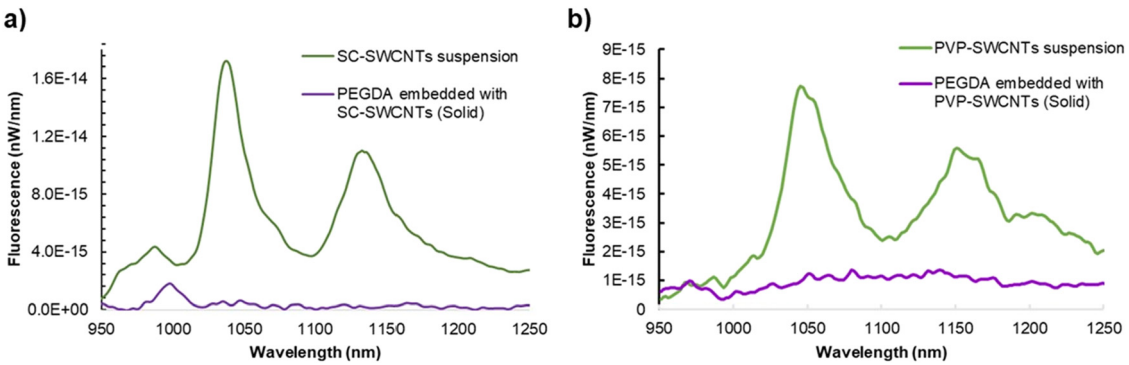

Fig. 4 Fluorescence measurements on SWCNT suspensions and printed solid structures; (a) SC-SWCNT suspension and the nanotube embedded PEGDA-based solid structure; (b) PVP-SWCNT suspension and the nanotube embedded PEGDA-based solid structure.

nanotubes in the PVP-SWCNT suspension was higher than that in the SC-SWCNTs to allow measurable photoluminescence from these samples under experimental conditions. In the next step, the photoinitiator (Irgacure 819 ~2.2 wt%) was added to the mixture and the mixture was briefly sonicated to allow homogenous mixing and *in situ* polymerization, and NIR fluorescence was measured. The results were analyzed to determine when SWCNT fluorescence was quenched. Both SC-SWCNTs and PVP-SWCNTs showed fluorescence quenching when the photoinitiator was added and the mixture was briefly sonicated (*ca.* 10 s) (Fig. S5). The formulation also turned into a solid polymer mass within minutes suggesting that sonication also facilitates the polymerization of acrylate in the presence of a radical initiator. During radical polymerization of PEGDA-based formulations, the decomposition of photoinitiator and the subsequent growth of acrylate radical chains generate a high localized concentration of free radicals ($R^{\bullet}$). It was suspected that free radicals/reactive oxygen species generated from the photochemical processes might have quenched the fluorescence. Under this situation, the quenching mechanism can proceed *via* photo-induced electron transfer (PET) and doping. Highly electrophilic reactive oxygen species (ROS) or specific radical intermediates can act as electron acceptors, withdrawing electron density from the SWCNT valence band. This p-type doping facilitates Auger recombination, where the exciton energy is transferred to an extra charge carrier, further suppressing radiative recombination.[17,51] However, the separation between the radical species and the nanotube surface can effectively insulate the SWCNT from radical-induced quenching. We found that the quenching effect appeared to be SWCNT-surface functionalization-dependent. Small molecule SC was unable to prevent photoluminescence quenching in the SWCNTs, which is consistent to similar observations reported in the literature that show emission can be quenched in SC-SWCNTs by reactive oxygen species (ROS).[7,51–53] Our results suggest that PVP may not provide an effective protective barrier for small radicals to reach the SWCNTs under the experimental conditions investigated in this research.

We then investigated an aromatic polymer, PS-*co*-PSS, a copolymer of styrene and styrene sodium sulfonate as a dispersant of SWCNTs. Polystyrene sodium sulfonate (PSS) helically wraps around the SWCNT, and both homopolymer (PSS) and copolymer PS-*co*-PSS form stable aqueous dispersions with SWCNTs.[53–55] PS-*co*-PSS functionalized SWCNTs preserved the characteristic SWCNT fluorescence within the PEGDA ink formulation and post sonication (Fig. 5a). The aromatic residues, styrene and its derivative which can act as radical scavengers, appear to provide necessary protection from quenching to the SWCNTs. Therefore, further experiments were performed using PS-*co*-PSS-SWCNTs integrated into 3D printing inks. Two types of structures, Flat and Truss (Fig. 1 and 5b), were printed by using a PS-*co*-PSS-SWCNT aqueous suspension (~130 mg L^{-1} nanotube concentration, initial concentration prior to mixing with printing ink) mixed with hydrogel 3D printing ink. NIR fluorescence was measured within the Flat and 3D Truss structures. The 3D Truss structure illustrates that SWCNTs can be incorporated into complex geometry objects, whereas the Flat structure facilitated the ease of fluorescence measurements. More importantly, both these 3D printed structures successfully maintained their characteristic fluorescence patterns (Fig. 5b). This finding shows that embedded SWCNTs can be successfully integrated within vat photopolymerization (DLP and CDLP printing methods) inks and be utilized for complex-shaped optical system development.

We observed that there is some difference in an apparent wavelength shift between the Flat and 3D Truss structures (Fig. 5b). This could arise due to potential differences in the crosslink densities on these structures which arise from differential volume/thickness of material exposed to photo-crosslinking during DLP. Previous study has shown that photoluminescence emission maxima shift as cross-linking is increased in SWCNTs embedded within a hydrogel.[25] Within crosslinked structures, the osmotic pressure could force conformational distortions in the polymer by rotating more polar groups to the nanotube surface, thereby changing the dielectric screening of the 1-D exciton and net PL changes.

SWCNT leaching tests

In order to evaluate whether the embedded SWCNTs within 3D-printed structures are retained over time, three hydrogel

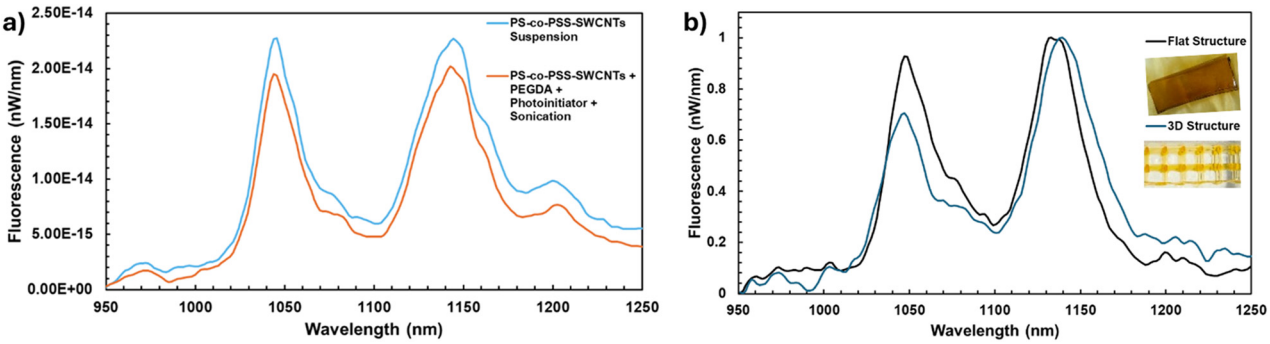

Fig. 5 (a) NIR fluorescence measurements of PS-*co*-PSS-SWCNTs in the suspension and after the steps for the formulation of the PEGDA ink (addition of crosslinker, photoinitiator, and sonication). (b) Normalized NIR emission of 3D printed structures – Flat and 3D Truss structures made with the Hydrogel 36–70 formulation, with embedded PS-*co*-PSS-SWCNTs.

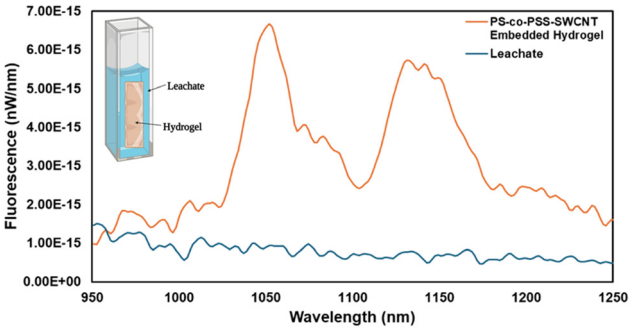

Fig. 6 NIR emission of the 10% PS-*co*-PSS hydrogel (3D printed Flat structure) compared to leachate to test for SWCNT leaching after 2 weeks in water.

samples were rinsed with DI water and soaked in DI water for 2 weeks. The solution was examined for characteristic SWCNT peaks after the structure was submersed in water for 2 weeks. The results (Fig. 6) show intrinsic photoluminescence from embedded SWCNTs, indicating that SWCNTs are retained within the printed structures under the examined conditions.

Mechanical properties (SWCNT-infused hydrogel composites)

For SWCNT-infused hydrogel ink suspensions, we used hydrogel 36–40, hydrogel 36–70, and Hydrogel 9–70 compositions. We also measured the mechanical properties of 20 vol% SWCNT mixed (PS-*co*-PSS) hydrogels and compared them with non-SWCNT infused hydrogels. We observed the mechanical properties of the SWCNT-infused hydrogel in both fragile (hydrogel 36–40) and durable (Hydrogel 36–70 and 9–70) inks to compare them with each other. The presence of SWCNTs could hinder the cross-linking efficiency of the ink formulation during the printing, potentially negatively affecting the measured mechanical properties.[56] The Hydrogel 36–40 hydrogel with functionalized SWCNTs showed lowered UTS (0.5 MPa) and Young's modulus (1.25 MPa) compared to the neat Hydrogel 36–40 (UTS – 0.54 MPa; Young's modulus 1.69 MPa), which is consistent with previous reports. However, the SWCNT-mixed Hydrogel 36–40 has slightly higher stretchability mainly due to lower crosslinking. Within the neat Hydrogel 36–70 and Hydrogel 9–70, the crosslinking is comparatively lower than the neat Hydrogel 36–40 (as shown *via* the measured mechanical properties in both Fig. 3b and 7b) due to higher water content in the ink. Based on the measured properties of the neat and SWCNT-infused hydrogels, the presence of SWCNTs appears to hinder the crosslinking, which reduces all the mechanical properties within the composite hydrogels, including stretchability and toughness (Fig. 7a). For example, Hydrogel 36–70 with SWCNTs showed an ~33.5% reduction in stretchability (62.78%) and a 56.4% reduction in toughness (59.77 kJ m^{-3}) compared to the neat Hydrogel 36–70 (stretchability: 94.43%; toughness: 137.15 kJ m^{-3}). Similarly, Hydrogel 9–70 with SWCNTs showed an ~40.6% reduction in stretchability (84.41%) and ~71.8% reduction in toughness (25.65 kJ m^{-3}) compared to the neat Hydrogel 9–70 (stretchability – 142%; toughness – 91.1 kJ m^{-3}). In terms of the tested SWCNT-infused hydrogels, the Hydrogel 9–70 formulation still maintained the highest stretchability, which maintains a similar trend as shown in the neat hydrogels. The Hydrogel 9–70 formulation is still the most useful for applications which may require more elastomeric behavior, but the significant reduction in stretchability due to SWCNT-infusion is noteworthy and will need to be taken into account.

Mechanical properties (varied concentrations of SWCNTs in the hydrogel composites)

The presence of SWCNTs in hydrogel ink clearly results in a reduction in the mechanical properties (Young's modulus and tensile strength) of the composites (Fig. 7). To delve more into the influence of SWCNTs in hydrogels, we characterized the mechanical properties of 5 vol% and 10 vol% SWCNT (PS-*co*-PSS) mixed Hydrogel 36–40 and compared them with those of the neat Hydrogel 36–40 (Fig. 8a and b). The increased concentration of SWCNT in the hydrogel composites does progressively lead to reduced key mechanical properties, indicating reduced crosslinking compared to the neat hydrogels under the same UV exposure conditions. For example, Young's

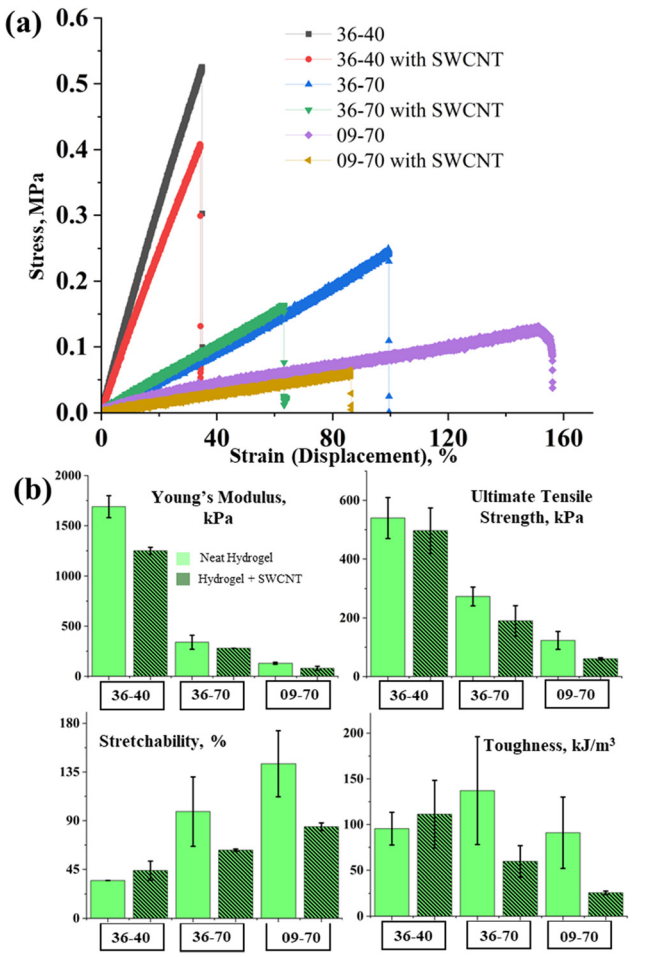

Fig. 7 (a) Stress–strain curve of the hydrogel compositions of 36–40, 36–70, and 9–70 with and without SWCNTs; (b) comparison of ultimate tensile strength, Young's modulus, stretchability and toughness in different hydrogel compositions with SWCNTs.

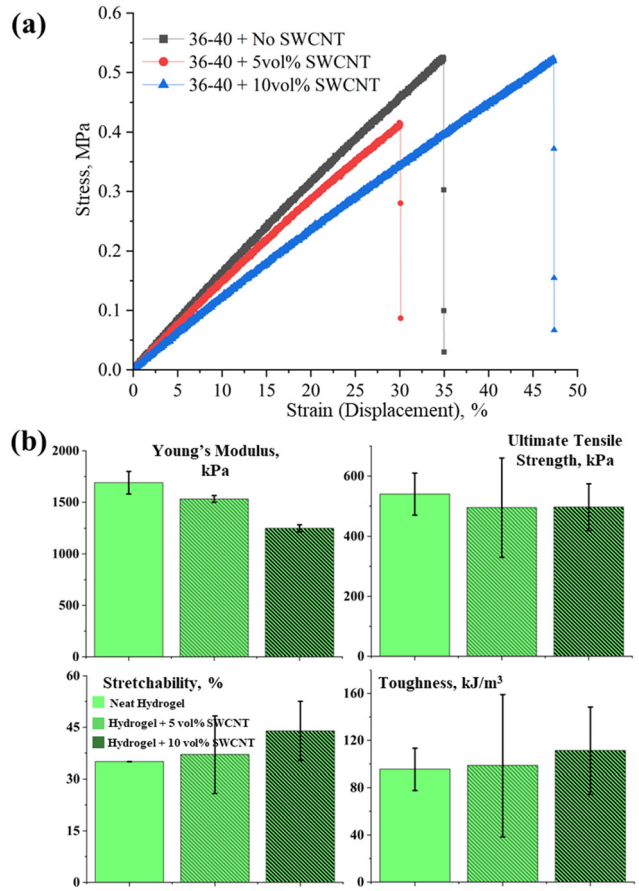

Fig. 8 (a) Stress–strain curve for the hydrogel composition 36–40 with variation in SWCNT concentration (0 vol%, 5 vol%, and 10 vol%); (b) comparison of ultimate tensile strength, Young's modulus, stretchability and toughness with different SWCNT concentrations.

modulus was reduced to 1.53 MPa with 5 vol% SWCNTs and 1.25 MPa with 10 vol% SWCNTs, compared to the value of 1.69 MPa for the neat hydrogel. Lower cross-linking with SWCNTs also increased the stretchability within the hydrogel composites. The stretchability was observed to be ~44% with 10 vol% SWCNTs and ~37% with 5 vol% SWCNTs, compared to the stretchability of ~35% exhibited by the neat hydrogel. Increases in SWCNT concentration also led to slight increases in the toughness of the hydrogel composite. The inclusion of SWCNTs into the ink likely acts as a secondary photo-absorber, in addition to the intentional photo-absorber Orasol Orange G dye. Both the Orasol Orange G and embedded SWCNTs then compete with the photoinitiator in absorbing the incident UV light, affecting the curing behavior. This increase in bulk stretchability can also account for the increased durability of the SWCNT-infused Hydrogel 36–40 samples.

FTIR characterization (Fig. S6) was additionally performed to gain insights on the effect of SWCNTs on polymerization (crosslinking) of all tested hydrogel formulations (neat and SWCNT-infused). Changes to the IR absorption peak corresponding to vinyl (C═C, double bond) is an indicator of the degree of crosslinking because this functionality will be converted to a C–C single bond during photopolymerization/crosslinking. Further analysis of the spectra showed that the solid cured SWCNT-infused hydrogels exhibited lower percentages of reduction in C═C double bonds than their neat hydrogel counterparts. This indicates a higher proportion of C═C bonds is still present within the final material under the same UV exposure conditions (Table S2). This illustrates and confirms there is less crosslinking within the SWCNT-infused hydrogels. The significant reductions in stretchability, tensile strength and toughness in the SWCNTs as observed in the high-water containing hydrogel formulations (Hydrogel 36–70 and Hydrogel 9–70) is indicative of a more complex interaction than just simple reduction in crosslinking. Potentially uneven dispersion of SWCNTs or additional nanoscale porosity could lead to premature failure in these hydrogel formulations. This will be the subject of further study.

Conclusions

In this work, we have successfully integrated functionalized photoluminescent SWCNTs within photocurable, 3D printable hydrogels. We demonstrated 3D fabrication of solid and lattice structures with functionalized SWCNT-based hydrogels *via* the CDLP printing process. Among different functionalization of SWCNTs with hydrogels, PS-*co*-PSS infused hydrogels showed promising responses in NIR fluorescence testing with no evidence of quenching which opens up their applications in NIR fluorescence based optical sensing platforms. Moreover, our developed hydrogel with different formulations exhibited adequate durability in multiple environmental conditions and tunable mechanical properties. High-water containing formulations Hydrogel 36–70 and Hydrogel 9–70 showed ''Highly Durable'' characteristics with no evidence of breakage after 48 hours in hydrated, dehydrated, or reversed conditions. Neat hydrogel 36–70 exhibited moderately high toughness (~137.15 kJ m^{-3}) and neat hydrogel 9–70 had the highest stretchability (~142%) among all formulations. The functionalized SWCNT-infused hydrogels resulted in reduced mechanical properties (Young's modulus, UTS, stretchability, and toughness) compared to the neat hydrogels, which is important to consider when selecting for an intended application. The inclusion of SWCNTs within these formulations did reduce stretchability and toughness, but the general trends shown in the neat hydrogels were maintained in the SWCNT-infused hydrogels. SWCNT-infused hydrogel 9–70 still maintained the highest stretchability (84.41%) compared to the other SWCNT-infused hydrogel formulations. In the future, the functionalized SWCNT-infused hydrogels will be implemented in the fabrication of different complex structures *via* a CDLP printing process for optical sensor development.

Author contributions

The manuscript was written through contributions of all authors. All authors have given approval to the final version of the manuscript.

Conflicts of interest

There are no conflicts to declare.

Data availability

The data supporting this article have been included as part of the Experimental section and supplementary information (SI). Supplementary information: Tables S1, S2 and Fig. S1–S6. See DOI: https://doi.org/10.1039/d6tb00108d.

Acknowledgements

The authors gratefully acknowledge the support provided by Wilson College of Textiles and College of Engineering at North Carolina State University. This work was supported by new faculty startup funds from Textile Engineering, Chemistry and Science Department (JBU), and from the Department of Mechanical and Aerospace Engineering (HOTW), Institute for Connected Sensor Systems (IConS) Seed Fund program (JBU and HOTW), North Carolina State University. We thank Xiaorui Guo for his assistance in FTIR data collection.

References

1 N. Yang, *et al.*, Carbon nanotube based biosensors, *Sens. Actuators, B*, 2015, **207**, 690–715.
2 E. Hemmer, *et al.*, Exploiting the biological windows: current perspectives on fluorescent bioprobes emitting above 1000 nm, *Nanoscale Horiz.*, 2016, **1**(3), 168–184.
3 N. Sultana, *et al.*, Understanding the Molecular Assemblies of Single Walled Carbon Nanotubes and Tailoring their Photoluminescence for the Next-Generation Optical Nanosensors, *Chem. Mater.*, 2024, **36**(9), 4034–4053.
4 S. Kruss, *et al.*, Carbon nanotubes as optical biomedical sensors, *Adv. Drug Delivery Rev.*, 2013, **65**(15), 1933–1950.
5 N. Karousis, N. Tagmatarchis and D. Tasis, Current progress on the chemical modification of carbon nanotubes, *Chem. Rev.*, 2010, **110**(9), 5366–5397.
6 P. W. Barone, *et al.*, Near-infrared optical sensors based on single-walled carbon nanotubes, *Nat. Mater.*, 2005, **4**(1), 86–92.
7 M. J. O'Connell, *et al.*, Reversible water-solubilization of single-walled carbon nanotubes by polymer wrapping, *Chem. Phys. Lett.*, 2001, **342**(3–4), 265–271.
8 M. Zheng, *et al.*, DNA-assisted dispersion and separation of carbon nanotubes, *Nat. Mater.*, 2003, **2**(5), 338–342.
9 V. C. Moore, *et al.*, Individually suspended single-walled carbon nanotubes in various surfactants, *Nano Lett.*, 2003, **3**(10), 1379–1382.
10 K. Yurekli, C. A. Mitchell and R. Krishnamoorti, Small-angle neutron scattering from surfactant-assisted aqueous dispersions of carbon nanotubes, *J. Am. Chem. Soc.*, 2004, **126**(32), 9902–9903.
11 H. M. Dewey, *et al.*, Carbon Nanotubes for Optical Detection of Quaternary Ammonium Compounds in Complex Media, *ACS Appl. Nano Mater.*, 2023, **6**(17), 15530–15539.
12 J. Budhathoki-Uprety, *et al.*, Helical polycarbodiimide cloaking of carbon nanotubes enables inter-nanotube exciton energy transfer modulation, *J. Am. Chem. Soc.*, 2014, **136**(44), 15545–15550.
13 J. Budhathoki-Uprety, *et al.*, Polymer cloaking modulates the carbon nanotube protein corona and delivery into cancer cells, *J. Mater. Chem. B*, 2017, **5**(32), 6637–6644.
14 C. Farrera, F. Torres Andón and N. Feliu, Carbon nanotubes as optical sensors in biomedicine, *ACS Nano*, 2017, **11**(11), 10637–10643.
15 M. J. O'connell, *et al.*, Band gap fluorescence from individual single-walled carbon nanotubes, *Science*, 2002, **297**(5581), 593–596.
16 C. Manzoni, *et al.*, Intersubband exciton relaxation dynamics in single-walled carbon nanotubes, *Phys. Rev. Lett.*, 2005, **94**(20), 207401.
17 H. M. Dewey, A. Lamb and J. Budhathoki-Uprety, Recent advances on applications of single-walled carbon nanotubes as cutting-edge optical nanosensors for biosensing technologies, *Nanoscale*, 2024, **16**, 16344–16375.
18 M. M. Safaee, M. Gravely and D. Roxbury, A wearable optical microfibrous biomaterial with encapsulated nanosensors enables wireless monitoring of oxidative stress., *Adv. Funct. Mater.*, 2021, **31**(13), 2006254.
19 M. Consales, *et al.*, Fiber Optic Chemical Nanosensors Based on Engineered Single-Walled Carbon Nanotubes: A Review, *J. Sens.*, 2008, **2008**(1), 936074.
20 N. D. Mansukhani, *et al.*, Optothermally Reversible Carbon Nanotube–DNA Supramolecular Hybrid Hydrogels, *Macromol. Rapid Commun.*, 2018, **39**(2), 1700587.
21 J. Zaumseil, Single-walled carbon nanotube networks for flexible and printed electronics, *Semicond. Sci. Technol.*, 2015, **30**(7), 074001.
22 R. Sharma, *et al.*, Single-wall carbon nanotubes based near-infrared sensors on flexible substrate, *2014 IEEE 11th International Multi-Conference on Systems, Signals & Devices (SSD14)*, Barcelona, Spain, 2014, pp. 1–5, DOI: 10.1109/SSD.2014.6808867.
23 M. Bordoni, *et al.*, 3D printed conductive nanocellulose scaffolds for the differentiation of human neuroblastoma cells, *Cells*, 2020, **9**(3), 682.
24 X. Wan, *et al.*, CNT-based electro-responsive shape memory functionalized 3D printed nanocomposites for liquid sensors, *Carbon*, 2019, **155**, 77–87.
25 P. W. Barone, *et al.*, Modulation of single-walled carbon nanotube photoluminescence by hydrogel swelling, *ACS Nano*, 2009, **3**(12), 3869–3877.
26 J. Budhathoki-Uprety, *et al.*, Synthetic molecular recognition nanosensor paint for microalbuminuria, *Nat. Commun.*, 2019, **10**(1), 3605.
27 J. Leijten, *et al.*, Spatially and temporally controlled hydrogels for tissue engineering, *Mater. Sci. Eng., R*, 2017, **119**, 1–35.
28 D. Chekkaramkodi, *et al.*, Review of vat photopolymerization 3D printing of photonic devices, *Addit. Manuf.*, 2024, **86**, 104189.
29 A. Zhang, *et al.*, 3D printing hydrogels for actuators: a review, *Chin. Chem. Lett.*, 2021, **32**(10), 2923–2932.
30 M. Saadi, *et al.*, Direct ink writing: a 3D printing technology for diverse materials, *Adv. Mater.*, 2022, **34**(28), 2108855.

31 Z. Zhu, H. S. Park and M. C. McAlpine, 3D printed deformable sensors, *Sci. Adv.*, 2020, **6**(25), eaba5575.
32 Y. Zhao, *et al.*, Long-term stability and durability of direct-ink-writing 3D-printed sensors: challenges, strategies and prospects, *Virtual Phys. Prototyping*, 2025, **20**(1), e2460211.
33 Q. Ge, *et al.*, Projection micro stereolithography based 3D printing and its applications, *Int. J. Extreme Manuf.*, 2020, **2**(2), 022004.
34 Z. Tang, *et al.*, Developments and Challenges in Direct Ink Writing for High-Performance Polymers, *Addit. Manuf. Front.*, 2025, **4**(2), 200218.
35 S. Subedi, *et al.*, Multi-material vat photopolymerization 3D printing: a review of mechanisms and applications, *npj Adv. Manuf.*, 2024, **1**, 9, DOI: 10.1038/s44334-024-00005-w.
36 T. Liu, *et al.*, Wireless wearable system based on multifunctional conductive PEG-HEMA hydrogel with antifreeze, anti-UV, self-healing, and self-adhesive performance for health monitoring, *Colloids Surf., A*, 2024, **695**, 134196.
37 C. Li, *et al.*, Polyelectrolyte elastomer-based ionotronic sensors with multi-mode sensing capabilities via multi-material 3D printing, *Nat. Commun.*, 2023, **14**(1), 4853.
38 H. Yan, *et al.*, 3D printing of dual cross-linked hydrogel for fingerprint-like iontronic pressure sensor, *Smart Mater. Struct.*, 2021, **31**(1), 015019.
39 Y. Zhang, *et al.*, Continuous 3D printing from one single droplet, *Nat. Commun.*, 2020, **11**(1), 4685.
40 S. Subedi, *et al*. Automated Grayscale Modulation to Enhance Digital Light Processing Fabrication Accuracy by Correcting Nonuniform Illumination, *J. Micro Nano Sci. Eng.*, 2025, **13**(2), 021001.
41 R. Chaudhary, *et al*., Additive manufacturing by digital light processing: a review, *Prog. Addit. Manuf.*, 2023, **8**(2), 331–351.
42 L. Wu, *et al.*, Bioinspired ultra-low adhesive energy interface for continuous 3D printing: reducing curing induced adhesion, *Research*, 2018, **2018**, 4795604.
43 H. O. T. Ware, R. Hai and C. Sun, Vat Photopolymerization, *Springer Handbook of Additive Manufacturing*, Springer, 2023, pp. 349–370.
44 P. J. Bártolo, *Stereolithography: materials, processes and applications*, Springer Science & Business Media, 2011.
45 M. Kwaśny, J. Polkowski and A. Bombalska, A Study on the Photopolymerization Kinetics of Selected Dental Resins Using Fourier Infrared Spectroscopy (FTIR), *Materials*, 2022, **15**(17), DOI: 10.3390/ma15175850.
46 ASTM D638-22, Standard Test Method for Tensile Properties of Plastics, 2022, ASTM International, West Conshohocken, PA, 2022.
47 M. Levin, *et al.*, Understanding the response of poly-(ethylene glycol) diacrylate (PEGDA) hydrogel networks: a statistical mechanics-based framework, *Macromolecules*, 2024, **57**(15), 7074–7086.
48 J. Shen, *et al.*, Effects of cross-link density and distribution on static and dynamic properties of chemically cross-linked polymers, *Macromolecules*, 2018, **52**(1), 121–134.
49 X. Li and J. P. Gong, Role of dynamic bonds on fatigue threshold of tough hydrogels, *Proc. Natl. Acad. Sci. U. S. A.*, 2022, **119**(20), e2200678119.
50 A. Lucantonio, *et al.*, Hydraulic fracture and toughening of a brittle layer bonded to a hydrogel, *Phys. Rev. Lett.*, 2015, **115**(18), 188105.
51 F. Sen, *et al.*, Observation of oscillatory surface reactions of riboflavin, trolox, and singlet oxygen using single carbon nanotube fluorescence spectroscopy, *ACS Nano*, 2012, **6**(12), 10632–10645.
52 H. Jin, *et al.*, Detection of single-molecule H_2O_2 signalling from epidermal growth factor receptor using fluorescent single-walled carbon nanotubes, *Nat. Nanotechnol.*, 2010, **5**(4), 302–309.
53 H. M. Dewey, *et al.*, Effect of Polyelectrolytes on the Photoluminescence of Single-Walled Carbon Nanotubes – Experimental and Simulation Studies, *ACS Omega*, 2025, **10**(11), 11474–11482.
54 P. Rama, *et al.*, Ion valence and concentration effects on the interaction between polystyrene sulfonate-modified carbon nanotubes in water, *J. Phys. Chem. C*, 2018, **122**(17), 9619–9631.
55 H. M. Dewey, *et al.*, Development of optical nanosensors for detection of potassium ions and assessment of their biocompatibility with corneal epithelial cells, *ACS Omega*, 2024, **9**(25), 27338–27348.
56 M. Bragaglia, *et al.*, 3D printing of biodegradable and self-monitoring SWCNT-loaded biobased resin, *Compos. Sci. Technol.*, 2023, **243**, 110253.